A High-Resolution UWB IR Superregenerative Receiver Front End With an SRD Quench Shaper

F. Xavier Moncunill-Geniz, Jordi Bonet-Dalmau, *Member, IEEE*, Pere Palà-Schönwälder, *Member, IEEE*, Francisco del Águila-López, and Rosa Giralt-Mas

***Abstract*—We present a simple receiver front end that makes use of the baseband superregeneration principle to detect ultra-wideband (UWB) impulse radio signals. The UWB antenna is directly connected to the core circuit consisting of a resistor-capacitor (RC) network coupled to a negative resistance that varies under the control of an external quench generator. Due to a step-recovery-diode quench shaper, 50-ps time-domain sensitivity windows are generated that filter the received pulses and reject noise and interference. The circuit achieves high gain, exhibits automatic gain control, and directly demodulates binary phase modulations.**

***Index Terms*—Circuit stability, impulse radio (IR), low-power design, radio receivers, step recovery diode (SRD), superregenerative receiver, ultrawideband (UWB) communication.**

I. Introduction

ULTRAWIDEBAND (UWB) technology has emerged as a promising means of achieving low complexity, low power, low cost, and high-data-rate connectivity for a variety of applications such as public safety, business, and consumer products. Impulse radio (IR) is a particular form of UWB signaling in which baseband pulses of extremely short duration (typically between 0.1 and 1.5 ns) are transmitted, thereby spreading the energy of the radio signal over a bandwidth of several gigahertz. UWB IR systems offer low complexity and low cost, have resistance to severe multipath and jamming, and achieve very good time-domain resolution in location and tracking applications [1].

Characterized by simplicity, low cost, and low power consumption, superregenerative receivers [2] have proven to be a good front-end solution in UWB IR communications [3]. In this brief, we present a very simple circuit suitable for the reception of UWB IR signals that can be understood as a baseband version of the superregenerative receiver. Palà-Schönwälder *et al.* [4] describe the principles of baseband superregeneration, whereas Moncunill-Geniz *et al.* [5] present the theory and an implementation adapted to generating and receiving subnanosecond pulses.

This brief presents, as a novelty, a complete receiver front end that includes a new baseband superregenerative amplifier (SRA) design, a step-recovery-diode (SRD) quench shaper, and a UWB antenna. The front end integrates the following functions in a simple and low-power structure: received-pulse windowing in the time domain, amplification with constant output amplitude, and direct demodulation of binary phase-shift keying (BPSK) pulse modulations. Due to the fast transitions of the signals generated by the SRD, both the time resolution and the RF bandwidth of the SRA are significantly improved.

Manuscript received August 24, 2011; revised November 9, 2011; accepted January 9, 2012. Date of current version February 23, 2012. This work was supported by the Spanish Dirección General de Investigación under Grant TEC2009-09924. This paper was recommended by Associate Editor A. Bevilacqua.

F. X. Moncunill-Geniz is with the Department of Signal Theory and Communications, Universitat Politècnica de Catalunya, 08034 Barcelona, Spain (e-mail: moncunill@tsc.upc.edu).

J. Bonet-Dalmau, P. Palà-Schönwälder, F. del Águila-López, and R. Giralt-Mas are with the Department of Electronic System Design and Programming, Universitat Politècnica de Catalunya, 08242 Manresa, Spain.

Color versions of one or more of the figures in this paper are available online at http://ieeexplore.ieee.org.

Digital Object Identifier 10.1109/TCSII.2012.2184373

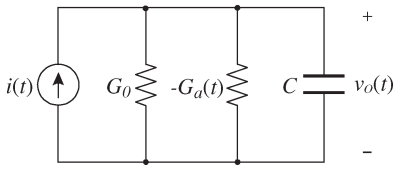

Fig. 1. Equivalent circuit model for the proposed SRA.

II. Principle of Operation

Fig. 1 shows the equivalent circuit model for the proposed SRA, where $i(t)$ represents the small signal injected by the antenna. It consists of an RC network coupled to a negative conductance that periodically varies under the control of an external quench generator. Let G_0 be the quiescent circuit conductance in its passive state, and let $-G_a(t)$ be the negative conductance generated by the active devices. The quench generator varies $G_a(t)$ so that the net conductance $G(t) = G_0 - G_a(t)$ becomes alternatively negative (producing a period of instability in which the capacitor voltage increases exponentially) and positive (producing a period of stability in which the voltage decreases exponentially). The voltage generated in a given quench cycle, i.e., of period T_q, depends on the input current $i(t)$ present in a certain sensitivity window or sensitivity period centered on the negative-slope zero crossing of $G(t)$ [5].

Let us define $R_0 = 1/G_0$ and $\tau_0 = R_0 C$. Let

$$i(t) = I p_c(t) \tag{1}$$

be an input current pulse, where I provides the pulse peak amplitude and polarity, and $p_c(t)$ is a unity-normalized shaping function [see Fig. 2(a)]. When the level of the signals generated in the circuit is low enough, the circuit operates in the linear mode. In this case, the response $v_o(t)$ to the input pulse $i(t)$

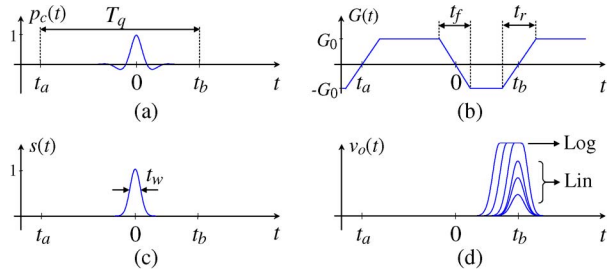

Fig. 2. SRA characteristic signals and functions. (a) Normalized input pulse $p_c(t)$. (b) Conductance function $G(t)$. (c) Sensitivity function $s(t)$. (d) Generated voltage $v_o(t)$ in the linear and logarithmic modes of operation.

under the assumptions considered in [5] is an amplified output pulse of the form

$$v_o(t) = IR_0K_rK_sp(t) \tag{2}$$

where $p(t)$ is the unity-normalized output pulse shape, K_r is the regenerative gain, which takes into account the input pulse shape, and K_s is the superregenerative gain, which is associated to the output exponential growth. K_s is the most significant amplification factor, with values typically exceeding 40 dB. In particular, the regenerative gain K_r can be calculated as

$$K_r = \frac{1}{\tau_0}\int_{t_a}^{t_b} p_c(\tau)s(\tau)d\tau \tag{3}$$

where $s(t)$ is the sensitivity function [see Fig. 2(c)] that, in the so-called slope-controlled state, can be approximated by a Gaussian expression dependent on the transition time t_f of $G(t)$ [see Fig. 2(b)] [5] as follows:

$$s(t) = e^{\frac{1}{C}\int_0^t G(\lambda)d\lambda} \approx e^{-\frac{1}{2}\left(\frac{t}{\sigma_s}\right)^2}, \qquad \sigma_s = \sqrt{\tau_0 t_f/2}. \tag{4}$$

To obtain maximum output amplitude, $s(t)$ needs to be properly aligned with $p_c(t)$. Therefore, a quench synchronization mechanism such as that described in [2] is required.

When the product $IR_0K_rK_s$ is high enough for the output voltage to reach saturation, the SRA operates in the logarithmic mode. In this case, as depicted in Fig. 2(d), the output amplitude remains constant, whereas the output pulsewidth depends on the logarithm of the input amplitude $|I|$. In our design, we have chosen this mode of operation because: 1) the output pulse amplitude is independent of the input amplitude, which provides a sort of automatic gain control, and 2) the output polarity is still determined by that of the input signal.

III. Reception of UWB IR Signals

Equation (2) shows that the amplified pulse generated at the output of the SRA $v_o(t)$ has the same polarity as the small-amplitude pulse $i(t)$ present at the input. Therefore, when the quench generator is properly synchronized, the SRA directly demodulates a BPSK pulse modulation, as shown in Fig. 3. Equation (3) shows that the SRA performs a time-domain filtering by windowing the input signal through $s(t)$ and that it effectively behaves as a sampler. The width of $s(t)$ at 60.7% of the maximum, i.e., $t_w = 2\sigma_s$, is a measure of the time

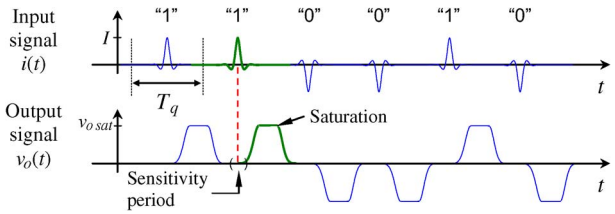

Fig. 3. SRA response to a UWB BPSK-modulated pulse train in the logarithmic mode.

resolution of the SRA [see Fig. 2(c)]. In our design, we aimed to minimize t_w to efficiently sample and amplify very short pulses. Equation (4) shows that narrow $s(t)$ may be achieved by reducing τ_0 and/or by reducing t_f. τ_0 may be reduced by lowering R_0, which leads to larger currents in the active devices, and/or by minimizing C, which is limited in practice by parasitic effects. In the current design, the capacitance was minimized by reducing the circuit layout size and by the choice of suitable active devices, and t_f was reduced by making use of an SRD to apply a fast-switching quench signal to the SRA.

IV. Implemented Front End

The physical implementation of the circuit in Fig. 1 is shown in Fig. 4 and consists of an SRD quench shaper, an SRA, and a symmetric bow-tie UWB antenna. The SRA uses a low-power and low-parasitic-capacitance cross-coupled BFR705L3RH transistor pair to generate the negative conductance. The parasitic transistor capacitance values are about 40% smaller than those in the previous design in [5]. The extremely small and flat leadless transistor package allows the circuit size to be minimized by creating a gap between the antenna terminals of only 0.5 mm. A relatively small value for the collector resistances $R_c = 22\ \Omega$ was selected to reduce R_0, whereas C in Fig. 1 is the overall parasitic capacitance at the antenna terminals. The lower transistor acts as a current source controlled by the SRD quench shaper. It controls the instantaneous bias current of the pair and, consequently, the degree of regeneration, in the form of negative resistance, which is generated in the SRA.

The SRD quench shaper takes advantage of the short transition times provided by SRDs under forward-bias conditions [6]. The quench generator signal, with relatively slow rising edges (1.8 ns), triggers the SRD-generating fast-rising edges (100 ps) at the output of the SRD quench shaper and, therefore, fast falling edges in $G(t)$. The fall time t_f of $G(t)$ is thus fixed by the SRD and independent of the quench generator rise time. The MMD837 SRD [7] requires a bias current of 1 mA to generate the 100-ps rise-time quench pulses. To reduce current consumption, the SRD is duty-cycled, with the bias control input activated to the 1.5-V supply voltage only when the quench generator pulse takes place.

The bow-tie antenna is suspended on a small portion of the circuit board to minimize the substrate (FR4) parasitic effects. As confirmed by experimental results in Section V, its length of 11.25 cm ensures that, in the transient regime (i.e., during the reception of a short pulse), it behaves as a resistive impedance, which validates the model in Fig. 1 with the antenna resistance included in R_0.

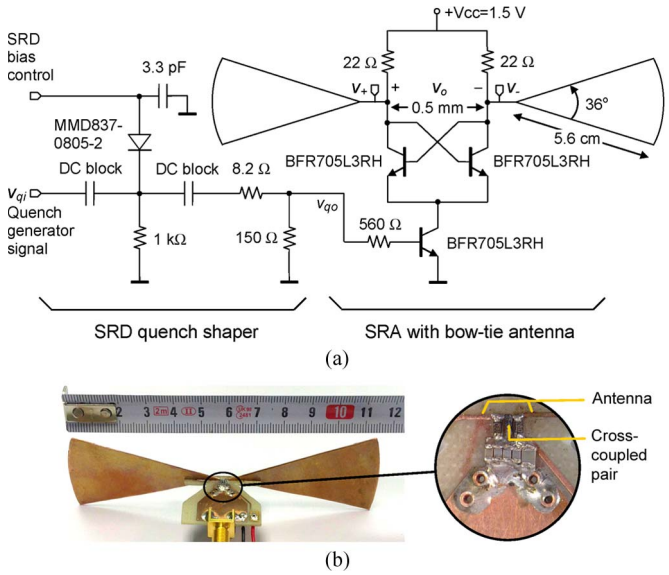

Fig. 4. (a) Schematic and (b) photograph of the implemented front end.

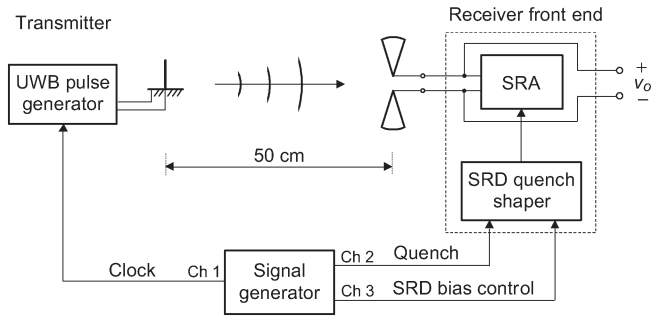

Fig. 5. Block diagram of the front-end test setup.

V. Measurement Results

Fig. 5 shows the block diagram of the implemented front-end test setup. The transmitter consists of a UWB pulse generator connected to a short monopole antenna on a ground plane. A signal generator drives both the transmitter and the receiver front end. This generator provides the SRD bias control and the quench signals with the proper delay to trigger the SRA at the desired instant. The voltage generated in the SRA (v_o) is measured by an Agilent 1169A active probe with a bandwidth of 12 GHz and capacitance of 0.21 pF.

We measured the S_{11} scattering parameter of a replica of the receiving antenna in Fig. 5. Fig. 6 shows the reflected voltage waveform calculated from the S_{11} parameter when a 1-V incident voltage step is applied to the bow-tie antenna. The plot exhibits three intervals. The first one corresponds to the delay introduced by the connector used to make the measure. In the second interval, the reflected waveform has a value of approximately 50% of the incident waveform. Therefore, the input impedance of the antenna in this interval is about 150 Ω. In the third interval, reflections from the end of the antenna arrive at the feeding point. Therefore, we conclude that the antenna behaves as a resistance of 150 Ω during 380 ps, which is a delay that corresponds to a distance of twice the length of one arm (5.6 cm × 2) and that largely exceeds the duration of the sensitivity period (50 ps) reported in the following. Note

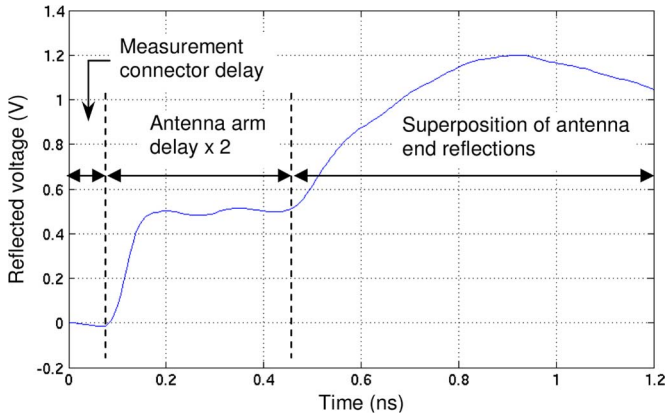

Fig. 6. Reflected waveform for a 1-V incident voltage step computed from the measured S_{11} parameter of a replica of the bow-tie antenna in Fig. 4.

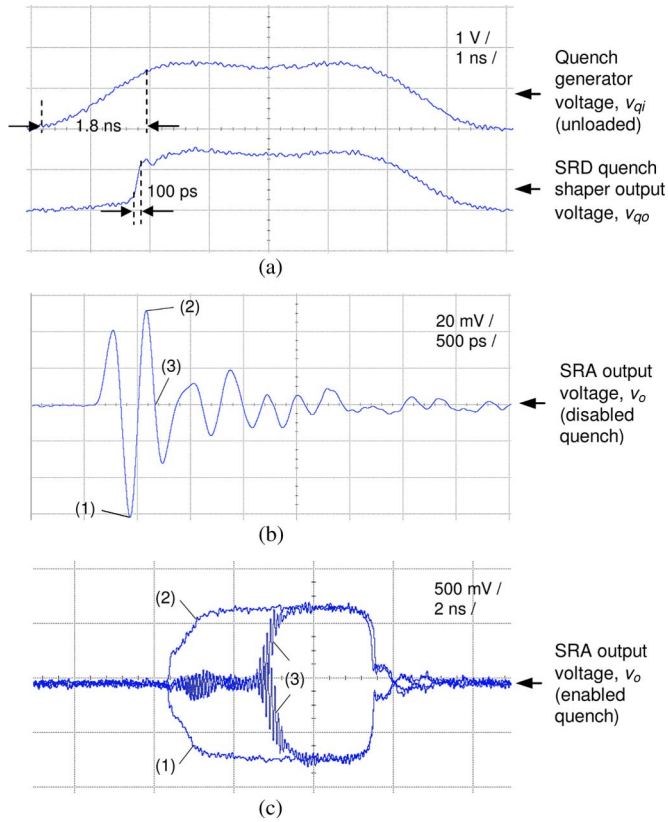

Fig. 7. (a) 100-ps rise-time pulse generated at the output of the SRD quench shaper from a quench generator pulse having a 1.8-ns rise time and a 5-ns width. (b) Signal generated at the receiver antenna terminals with the quench disabled when a 100-ps rise-time step is applied to the transmitting antenna. (c) Pulses generated in the SRA with the quench enabled (logarithmic mode) when sampling (1) at a minimum, (2) at a maximum, and (3) at a zero crossing of the signal in (b). All screenshots were taken at 40 Gsample/s and with a bandwidth of 12 GHz.

that given the small value of the collector resistances in Fig. 4 $(R_c = 22\ \Omega)$, the antenna resistance plays a secondary role in determining R_0.

Fig. 7 shows the different signals measured at the receiver front end. Results show that, upon reception of a UWB impulse, the SRA generates relatively large-amplitude and wide output pulses whose polarity is controlled by that of the input signal. As confirmed by this measurement, the SRA is able to

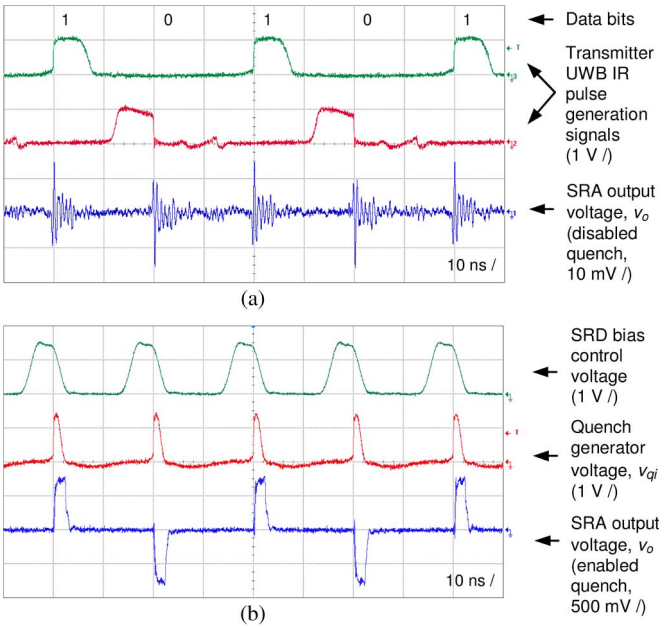

Fig. 8. (a) Signals at the transmitter and receiver sides when transmitting a UWB IR BPSK modulation and (b) corresponding signals at the receiver front end during reception.

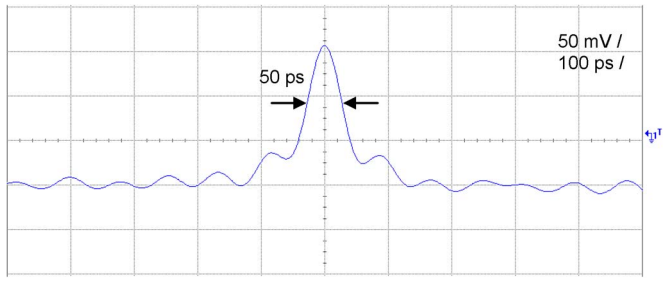

Fig. 9. Pulse generated in the SRA in the linear mode.

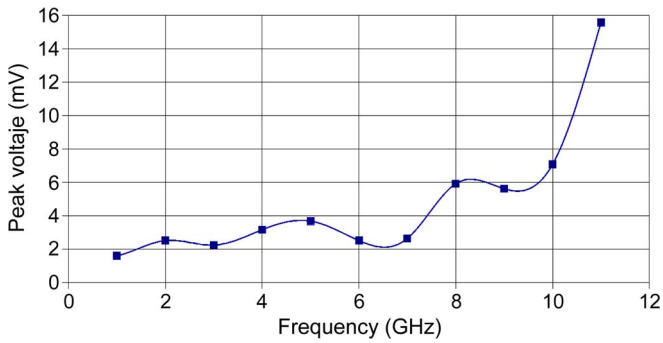

Fig. 10. Sensitivity to a CW signal (10^{-3} error rate in output pulse polarity).

discriminate the input polarity within very short time intervals (< 180 ps). Therefore, when the quench generator is properly synchronized to sample a lobe of the input pulses, the SRA directly demodulates a BPSK modulation, as verified in Fig. 8. For the generation of the BPSK modulation, the transmitter combines two signals: the first one controls the generation of positive polarity UWB IR pulses by generating 100-ps rise-time pulses, whereas the second one controls the generation of negative polarity pulses by generating 100-ps fall-time pulses. These two signals, shown in Fig. 8(a), are combined (added) and sent through the transmitting antenna. The corresponding pulses measured at the receiver antenna terminals with the quench disabled are also shown in Fig. 8(a). Fig. 8(b) shows the front-end control signals and the response of the SRA to the BPSK modulation with the quench enabled. The pulse rate is 50 Mpulse/s, the SRD bias control signal operates with a 30% duty cycle, the quench generator pulsewidth is 2 ns, and the pulses generated in the SRA follow the input-signal polarity with a peak-to-peak amplitude of 1.5 V. The SRA supports quench frequencies up to 250 MHz. However, the maximum pulse rate in the current setup is quite lower because of the intersymbol interference created by the actual pulses measured at the receiving antenna [Fig. 8(a)].

Fig. 9 shows a pulse generated in the SRA in the linear mode, which was obtained by decreasing the quench generator pulsewidth to reduce gain. As derived from [5], the pulses generated in the linear mode give an estimate of the actual sensitivity function, whose width is, in this case, $t_w \approx 50$ ps. This value estimates the sampling resolution of the SRA, which represents an improvement of one order of magnitude with respect to the 500 ps of the previous design in [5] and sets a landmark value for this type of receiver. We measured $t_w \approx 200$ ps without the use of the SRD quench shaper. This means that the resolution improvement factor due to the new SRA design is of about 2.5, whereas the SRD quench shaper introduces an improvement factor of approximately 4. According to (3), the quench generator jitter has to be small compared with the width of the sampled pulse lobe.

Fig. 10 shows the sensitivity of the SRA to a continuous-wave (CW) signal in the range of 1–11 GHz. In this measurement, the sensitivity periods were centered on the lobes of the received sine wave, and the amplitude of the transmitted signal was adjusted to yield an error rate of 10^{-3} in the output pulse polarity. The peak sensitivity value (voltage measured at the antenna terminals after deactivation of the quench generator) was between 2 and 4 mV in the range of 2 to 7 GHz, it rose to 7 mV at 10 GHz, and it rapidly increased beyond that frequency. Note that a voltage of 2 mV during 50 ps on an impedance of 50 Ω represents an average power of about -84 dBm at 1 Mpulse/s, which is a value that is comparable to typical receiver sensitivities. The bandwidth at -10 dB that results from the measurements in Fig. 10 is about 8 GHz.

Table I summarizes the main front-end features, and Table II makes a comparison with recent UWB IR receiver architectures. The RF bandwidth of the current design is extremely large, and the power consumption and the energy efficiency (excluding the quench generation and synchronization circuitry, with a consumption typically on the order of that of the SRA [2]) is in line with the state of the art.

VI. Conclusion

We present a new superregenerative receiver front end for communications and ranging where a baseband SRA controlled by an SRD quench shaper behaves as a high-resolution time-domain filter and amplifier, suitable to the reception of pulses in the range of 3.1–10.6 GHz defined by the UWB spectrum

TABLE I
SUMMARY OF FRONT-END PERFORMANCE ($V_{cc} = 1.5$ V, QUENCH GENERATOR PULSE WIDTH = 2 ns)

Parameter	1 Mpulse/s	50 Mpulse/s
SRA sensitivity function width, t_w	~ 50 ps	
SRA peak-to-peak output voltage	1.5 V	
SRA peak voltage gain at sensitivity level	~ 50 dB	
Supply current		
SRD quench shaper (duty cycle)	40 µA (4 %)	0.3 mA (30 %)
SRA	140 µA	1.9 mA
Total	180 µA	2.2 mA
Total power consumption	0.27 mW	3.3 mW

TABLE II
COMPARISON OF UWB IR RECEIVER PERFORMANCE

	Operating frequency (GHz)	Bandwidth (GHz)	Pulse rate (Mpulse/s)	Power (mW)	Energy per pulse (pJ/pulse)
[8] (1)	1.9	0.0005	0.005	0.4	80000
[2] (1)	2.4	0.064	11	2.1	190
[9]	3.5 - 4.5	0.5	16	22.5	1400
[10]	0.625	0.5	39	2.7	70
[11]	7.25 - 8.5	0.3 - 0.85	112	5.4	48
[12]	7.6	1.25	5	4.2	840
This work	Baseband	8	50	3.3	66

(1) Narrowband superregenerative receiver

mask. The SRA exhibits extremely large bandwidth and directly converts a BPSK modulation in the range of millivolts into a 1.5-V peak-to-peak return-to-zero pulse train. Reception of ON-OFF keying and pulse position modulations is also feasible by detecting the output pulsewidth. Unlike bandpass superregenerative receivers, this proposal requires no envelope detector, which contributes to higher front-end simplicity and lower power consumption.

ACKNOWLEDGMENT

The authors would like to thank Altaix Electrónica S.A.L. for supplying the SRD samples free of charge.

REFERENCES

[1] I. Oppermann, M. Hämäläinen, and J. Iinatti, *UWB Theory and Applications*. Chichester, U.K.: Wiley, 2004.

[2] F. X. Moncunill-Geniz, P. Palà-Schönwälder, C. Dehollain, N. Joehl, and M. Declercq, "An 11-Mb/s 2.1-mW synchronous superregenerative receiver at 2.4 GHz," *IEEE Trans. Microw. Theory Tech.*, vol. 55, no. 6, pp. 1355–1362, Jun. 2007.

[3] M. Pelissier, D. Morche, and P. Vincent, "Super-regenerative Architecture for UWB pulse detection: From theory to RF front-end design," *IEEE Trans. Circuits Syst. I, Reg. Papers*, vol. 56, no. 7, pp. 1500–1512, Jul. 2009.

[4] P. Palà-Schönwälder, F. X. Moncunill-Geniz, J. Bonet-Dalmau, F. del-Águila-López, and R. Giralt-Mas, "Baseband superregenerative amplification," *IEEE Trans. Circuits Syst. I, Reg. Papers*, vol. 52, no. 9, pp. 1930–1937, Sep. 2009.

[5] F. X. Moncunill-Geniz, P. Palà-Schönwälder, J. Bonet-Dalmau, F. del Águila-López, and R. Giralt-Mas, "Sub-nanosecond pulse filtering and amplification through first-order controlled circuit instability," in *Proc. 39th Eur. Microw. Conf.*, Rome, Italy, Sep. 29–Oct. 1, 2009, pp. 1319–1322.

[6] Hewlett-Packard, Application Note 918 Pulse and Waveform Generation with Step Recovery Diodes. [Online]. Available: http://www.hp.woodshot.com/hprfhelp/lit/diodelit.htm

[7] Aeroflex-Metelics, Silicon Step Recovery Diodes Datasheet. [Online]. Available: http://www.aeroflex.com/ams/Metelics/pdfiles/Step_Recovery_Diodes_SRD_A17037.pdf

[8] B. Otis, Y. H. Chee, and Y. Rabaey, "A 400 μW-RX, 1.6mW-TX superregenerative transceiver for wireless sensor networks," in *Proc. IEEE Int. Solid-State Circuits Conf. Dig. Tech. Papers*, San Francisco, CA, Feb. 2005, vol. 1, pp. 396–606.

[9] D. C. Daly, P. P. Mercier, M. Bhardwaj, A. L. Stone, Z. N. Aldworth, T. L. Daniel, J. Voldman, J. G. Hildebrand, and A. P. Chandrakasan, "A pulsed UWB receiver SoC for insect motion control," *IEEE J. Solid-State Circuits*, vol. 45, no. 1, pp. 153–166, Jan. 2010.

[10] N. Van Helleputte and G. Gielen, "A 70 pJ/pulse analog front-end in 130 nm CMOS for UWB impulse radio receivers," *IEEE J. Solid-State Circuits*, vol. 44, no. 7, pp. 1862–1871, Jul. 2009.

[11] M. Pelissier, J. Jantunen, B. Gomez, J. Arponen, G. Masson, S. Dia, J. Varteva, and M. Gary, "A 112 Mb/s full duplex remotely-powered impulse-UWB RFID transceiver for wireless NV-memory applications," *IEEE J. Solid-State Circuits*, vol. 46, no. 4, pp. 916–927, Apr. 2011.

[12] S. Solda, M. Caruso, A. Bevilacqua, A. Gerosa, D. Vogrig, and A. Neviani, "A 5 Mb/s UWB-IR transceiver front-end for wireless sensor networks in 0.13 μm CMOS," *IEEE J. Solid-State Circuits*, vol. 46, no. 7, pp. 1636–1647, Jul. 2011.